Triangular SOS models and cubic-crystal shapes

1984 J. Phys. A: Math. Gen. 17 3559

(http://iopscience.iop.org/0305-4470/17/18/025)

J. Phys. A: Math. Gen. 17 (1984) 3559-2581. Printed in Great Britain

Triangular SOS models and cubic-crystal shapes

B Nienhuis†, H J Hilhorst‡ and H W J Blöte‡

† Philips Natuurkundig Laboratorium, Postbus 80.000, 5600 JA Eindhoven, The Netherlands

‡ Laboratorium voor Technische Natuurkunde, Postbus 5046, 2600 GA Delft, The Netherlands

Received 22 June 1984

Abstract. A solid-on-solid model in a field $\hat{h}$ conjugate to the orientation of the surface is exactly solved with the aid of Pfaffians. The free energy $f(\hat{h})$ directly gives the equilibrium shape of a finite crystal. The phase diagram exhibits rough and smooth phases, corresponding to rounded and flat portions of the crystal surface. The solid-on-solid model undergoes transitions of the Pokrovsky–Talapov type characterised by a specific heat exponent $\alpha = \frac{1}{2}$. One special point of the phase diagram corresponds to the appearance of a facet via an $\alpha = 0$ transition. Height–height correlations are derived along a special line in the phase diagram. With the aid of the known equivalence of this SOS model with an Ising model, several exponents can be translated from one model to the other. This enables us to derive the topology of the phase diagram of the antiferromagnetic triangular Ising model with first- and second-neighbour couplings in a field.

1. Introduction

Solid-on-solid (SOS) models describe the roughening transition of crystal surfaces and are also relevant for the description of the equilibrium shape of finite crystals. The connection to crystal shapes has recently been reviewed by Rottman and Wortis (1984) and Zia (1983). In summary, if one can find the free energy $g(\hat{m})$ of an SOS model which is constrained to a given average spatial orientation $\hat{m}$ with respect to the crystal axes, then the shape of the corresponding crystal can be obtained via the Wulff (1901) construction. This construction, recently reinterpreted by Andreev (1981) as a Legendre transformation, follows from minimising the total surface free energy at constant volume. Several interesting consequences of the relation between SOS models and crystal shapes have been pointed out by Jayaprakash *et al* (1983), who performed explicit calculations in the BCSOS model (van Beijeren 1977).

Only a few SOS models can be solved exactly. It is therefore of importance to extract, from those that can be solved, the maximum of knowledge about the shape of finite crystals. Here we investigate a system introduced by Blöte and Hilhorst (1982), which is probably the simplest exactly solvable non-trivial SOS model. It is particularly suited to study the shape of the (1, 1, 1) corner of a simple cubic crystal. The relative simplicity of this system is due to the fact that all its properties can be translated directly into the properties of a zero-temperature Ising antiferromagnet on the triangular lattice. For this reason we shall henceforth refer to this system as the TISOS (for 'Triangular' and 'Ising') model. Utilising the Ising equivalence, Blöte and Hilhorst obtained, among other results, the free energy $f(\hat{h})$ for the TISOS model, where $\hat{h}$ *is a*

0305-4470/84/183559+23$02.25

field which couples to the surface gradient. It follows from the arguments by Andreev and by Rottman and Wortis that this $f(\hat{h})$ directly represents the shape of a finite crystal, $\hat{h}$ corresponding to a spatial direction. The TISOS model implies a rounding of the (1, 1, 1) corner of a simple cubic crystal, as well as a sharp boundary line between the rounded part of the surface and the facets parallel to the three main crystal planes (see figure 1). Near this boundary, the tangent to the surface approaches the orientation of the facet with a characteristic power $\frac{1}{2}$. This power follows directly from the specific heat exponent α of the corresponding zero-temperature Ising model, which has the remarkable value $\alpha = \frac{1}{2}$.

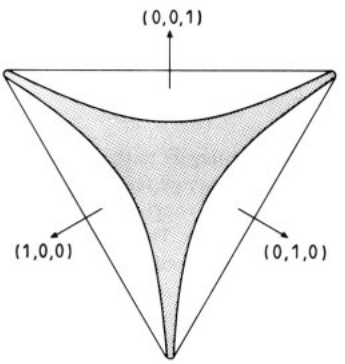

Figure 1. Equilibrium crystal shape according to the TISOS model solved by Blöte and Hilhorst (1982). The crystal is shown in a projection parallel to the (1, 1, 1) direction. The shaded area represents the curved part of the crystal surface, and the three remaining areas indicate the (1, 0, 0), (0, 1, 0) and (0, 0, 1) facets.

In this paper we study the TISOS model with additional interactions: these interactions favour surface flattening (facet formation) parallel to the (1, 1, 1) plane. It is nevertheless amenable to exact analysis. As a consequence, by varying the interactions we can study the formation of the (1, 1, 1) facet, and several other properties of the finite-crystal shape. The appearance of this facet is a transition not in the Kosterlitz–Thouless (1973) universality class.

This paper is organised as follows. In § 2 we briefly review the correspondence between the configurations of an SOS model and those of an Ising antiferromagnet on a triangular lattice in its ground state. We also recall the relation between the SOS free energy and crystal shapes. In § 3 we define an SOS Hamiltonian with three different couplings in a field $\hat{h}$. We then solve the equivalent Ising problem at temperature $T_{Is} = 0$, by means of Pfaffians. In § 4, we discuss the resulting phase diagram for the TISOS model. Several transitions between rough and smooth phases are found. We simplify the expressions for the free energy of the smooth phases and find the critical behaviour along the critical lines. These results are interpreted in terms of the equilibrium shape of the (1, 1, 1) corner of a cubic crystal and its behaviour near the point of facet formation.

In § 5 we calculate the height–height correlation function for the TISOS model in some spatial directions in representative regions of the phase diagram.

In § 6 we find the correspondence between spin-wave and vortex operators in the TISOS model, on the one hand, and temperature and magnetic field operators in the Ising antiferromagnet on the other hand. The exponents of these operators are derived.

A new result for the Ising model is that in the antiferromagnetic ground state the magnetic field $H = B/k_B T_{Is}$ is irrelevant, i.e. there is a non-vanishing range of H for which the system remains critical. This explains a somewhat surprising numerical result for the location of the critical line in the B–T plane by Kinzel and Schick (1981). When a ferromagnetic second-neighbour interaction is turned on, the Ising antiferromagnet on a triangular lattice orders in a state characterised by six-fold symmetry. This model is believed to be in the same universality class as the six-state clock model, which possesses a massless intermediate phase. In § 7 we discuss qualitatively the expected phase diagram of the TISOS model in the presence of such a second-neighbour interaction. A brief discussion of our main results is given in § 8.

2. Ising, dimer and SOS models, and the cubic-crystal shape

The behaviour of the nearest-neighbour triangular Ising antiferromagnet is dominated by the circumstance that not all pairs of interacting spins can be antiparallel. Each elementary triangle is frustrated, because at least two of its spins must be of the same sign. If all Ising interactions are exactly equal, the ground state of such a model is infinitely degenerate. In this section we will describe a correspondence between the degrees of freedom that remain in this ground state, and the degrees of freedom of an SOS model on the triangular lattice. There is a convenient way to visualise this correspondence.

At zero Ising temperature (if boundary conditions allow, which we shall assume), each elementary triangle will contain two bonds between antiparallel spins and one between parallel spins. If one erases all lattice edges between parallel spins, one obtains a plane filled with rhombi or diamonds (figure 2). Such a diamond covering can also be interpreted as the irregular surface of a truncated simple cubic lattice, viewed from the (1, 1, 1) direction. The apparent heights are precisely the possible configurations of the TISOS model. The correspondence between allowed Ising configurations and diamond coverings has another useful consequence. Each rhombus can be associated with a dimer on the dual lattice. Hence these Ising and SOS models are also equivalent to a dimer model on the honeycomb lattice, the problem being to cover the entire lattice with dimers in such a way that each site is the end point of precisely one dimer. These dimer models can be solved directly with the aid of Pfaffians.

For a more precise description of the mappings of Ising onto SOS configurations, we divide the elementary triangles of the lattice into two kinds: those pointing to the

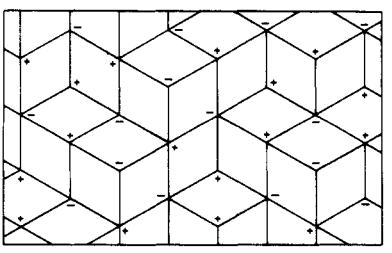

Figure 2. Illustration of the mapping of a zero-temperature Ising configuration onto a diamond or dimer configuration. A diamond configuration is obtained by erasing all edges of the triangular lattice which connect parallel spins.

right and those pointing to the left. We assign height differences between the sites of the triangular lattice as follows. Going clockwise along the edges of each triangle pointing to the right, we associate a height increment +1 with the edges connecting antiparallel spins, and an increment −2 with those connecting parallel spins. An equivalent procedure to find these height increments is to use the triangles pointing to the left and to follow a counterclockwise path. This is illustrated in figure 3. It is obvious that the sums of the height increments vanish along elementary triangles, and consequently along all closed paths. Hence height differences between two sites of the triangular lattice do not depend on the path chosen for its determination. Furthermore, if we fix the value of a height variable n_i at site i, say $n_i = 0$, then all other height variables n_j follow directly from a given ground state Ising configuration. SOS configurations obtained in this way are subject to the following restrictions.

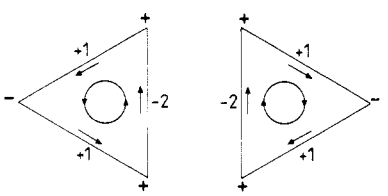

Figure 3. SOS height differences as obtained from zero-temperature Ising configurations. Height increments +1 and −2 are assigned to bonds between antiparallel spins and parallel spins respectively. In order to obtain the sign of the height differences, the paths along which the increments are defined are clockwise and counterclockwise for the two triangle orientations shown. Thus the sign of each height difference becomes independent of the choice of the triangle for its determination.

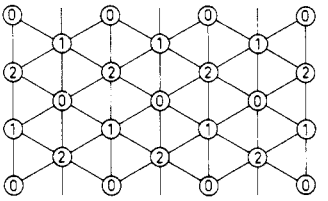

Figure 4. Division of the triangular lattice into three triangular sublattices. We have labelled the sublattices such that the height variables on sublattice i ($i = 0, 1, 2$) are equal to i plus a multiple of 3.

(1) As shown in figure 4, the height variables modulo 3 on each of the three sublattices only assume the values 0, 1, and 2, respectively.

(2) Height differences $|n_i - n_j|$ between nearest neighbours i and j do not exceed 2. Conversely, from each SOS configuration subject to these restrictions, one can obtain an Ising configuration by requiring that odd and even height variables correspond to spins of different sign. If we fix the value of a given Ising spin, then the values of all other Ising spins follow. Furthermore, it is easily checked that this Ising configuration obeys the $T = 0$ antiferromagnetic constraint that no elementary triangle should contain three spins with equal signs. Hence, there is a one-to-one correspondence between allowed Ising and TISOS configurations if one site variable is fixed in each model.

The SOS free energy models the thermodynamics of the surface of a crystal. The shape of the crystal can be found from the condition that this free energy be minimal. The minimisation procedure results in a remarkably simple relation between the surface free energy and the crystal shape. This relation was found recently by Andreev (1981). Since it plays an important rôle in this paper, we derive it again below.

The shape of a crystal can be written as an equation of the form

$$r_3 = S(r_1, r_2), \tag{2.1}$$

where r_1, r_2 and r_3 are the coordinates of points on the surface. For the entire crystal S is a double-valued function, but we may deal with one branch at a time. The orientation of the crystal surface, $\hat{m}$, is the directon of the vector $\boldsymbol{m} = (m_1, m_2, -1)$, with

$$m_j = \partial S(r_1, r_2)/\partial r_j \qquad \text{with } j = 1, 2. \tag{2.2}$$

The shape S minimises the total surface free energy

$$F = \int \tilde{g}(m_1, m_2)\, \mathrm{d}r_1\, \mathrm{d}r_2, \tag{2.3}$$

for fixed values of the volume

$$V = \int S(r_1, r_2)\, \mathrm{d}r_1\, \mathrm{d}r_2. \tag{2.4}$$

Here the surface free energy density $g(\hat{m}) = \tilde{g}(m_1, m_2)/|\boldsymbol{m}|$, and m_i are implicit functions of r_j through (2.2). The corresponding Lagrange equation is

$$\frac{\mathrm{d}}{\mathrm{d}r_j}\frac{\partial \tilde{g}(m_1, m_2)}{\partial m_j} = \frac{\partial m_i}{\partial r_j}\frac{\partial^2 \tilde{g}(m_1, m_2)}{\partial m_i\, \partial m_j} = 2\lambda, \tag{2.5}$$

where λ is a Lagrange multiplier and summation from 1 to 2 over doubly occurring indices is understood. The Legendre transform of the crystal shape S is a function of the same arguments as $\tilde{g}$:

$$T(m_1, m_2) = m_j r_j - S(r_1, r_2). \tag{2.6}$$

As a consequence it is more straightforward to solve (2.5) for T and find the crystal shape from it. Note that the following expression follows identically from the definition of T

$$\partial r_i/\partial m_j = \partial^2 T(m_1, m_2)/\partial m_i\, \partial m_j. \tag{2.7}$$

Therefore an obvious solution of (2.5) is

$$T(m_1, m_2) = \tilde{g}(m_1, m_2)/\lambda. \tag{2.8}$$

Though we do not know the general solution of the Lagrange equation, it appears that (2.8) is the physically significant solution. Hence

$$S(r_1, r_2) = m_j r_j - \tilde{g}(m_1, m_2)/\lambda, \tag{2.9}$$

which looks much like the Legendre transform of $\tilde{g}(m_1, m_2)$, as already suggested by (2.8). Indeed if we introduce

$$f(h_1, h_2) = h_j m_j - \tilde{g}(m_1, m_2)$$

with

$$h_j = \partial \tilde{g}(m_1, m_2)/\partial m_j, \tag{2.10}$$

then from (2.8)

$$h_j = \lambda r_j$$

and

$$S(r_1, r_2) = f(\lambda r_1, \lambda r_2)/\lambda. \tag{2.11}$$

This $f(h_1, h_2)$ is the interfacial free energy as a function of the fields conjugate to the gradient of the crystal surface. Hence the shape of the crystal itself is a three-dimensional plot of its interface free-energy density. The value of λ in (2.11) is determined by the constraint (2.4).

3. The TISOS model and its solution

We shall now assign energies to the configurations described in the previous section. The energy of a pair of neighbouring sites i and j depends only on the height variables n_i and n_j on these sites. We shall describe the interaction between these sites by coupling strength parameters K_{ij} chosen such that the reduced energy (energy divided by $k_B T$) of a pair of nearest neighbours is K_{ij} if the height difference $|n_i - n_j|$ is 2, and $-K_{ij}$ if the height difference is 1. Hence

$$H_{\mathrm{SOS}} = -\sum_{\langle ij \rangle} K_{ij}(3 - 2|n_i - n_j|). \tag{3.1}$$

The sum is over all pairs of nearest neighbours (i, j), each pair being counted once. One possibility is to let the K_{ij} depend only on the direction of the bond $\langle ij \rangle$. Then $K_{ij} \in \{h_1, h_2, h_3\}$, the h_μ being defined in figure 5. Such couplings have the character of a field coupling to the average slope of the SOS surface. To make this clear we may describe the nearest-neighbour height differences by a discrete gradient vector $\nabla n_i = (n_{i+e_1} - n_i, n_{i+e_2} - n_i, n_{i+e_3} - n_i)$. Here the e_l are three unit vectors on the triangular lattice at angles of $2\pi/3$, chosen such that each of the three components of ∇n_i can only take the values -2 or $+1$. It is then possible to verify that (3.1) can be cast in the

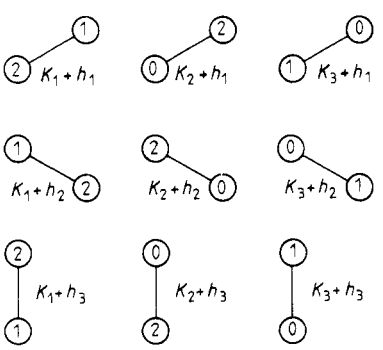

Figure 5. Definition of the coupling strengths of the TISOS model considered in this work. The interactions depend on the orientation of the bond as well as on the labels of the sublattices connected by the bond. For $K_i = 0$, we get the couplings discussed following equation (3.1).

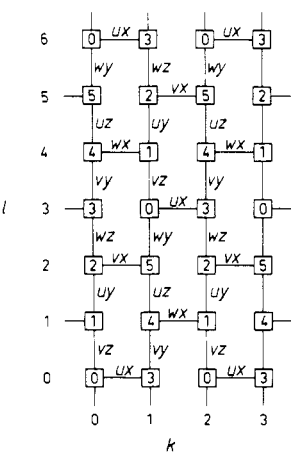

Figure 6. Dimer weights in terms of the fugacities defined in equation (3.3). In order to allow easy site labelling with integer coordinates (k, l), the honeycomb lattice is deformed to a brick lattice. The sites of this lattice can be divided into six types as indicated. Sites with the same type number are connected by translational invariance of the Hamiltonian.

equivalent form

$$H_{\mathrm{SOS}} = \tfrac{1}{3}N_s(h_1+h_2+h_3) - \tfrac{2}{3}\sum_i \boldsymbol{h}\cdot\nabla n_i \tag{3.2}$$

where N_s is the total number of sites. This anisotropic model was investigated recently (Blöte and Hilhorst 1982). It was exactly solved via the equivalence with the zero-temperature triangular Ising antiferromagnet. For sufficiently strong field anisotropy, the system locks into a configuration with the maximum slope allowed by the constraints (all dimers in the same orientation in figure 4). This transition has a specific heat exponent $\alpha = \frac{1}{2}$, in contrast to the usual roughening transition for which $\alpha = -\infty$. The ground state does not allow local excitations, only above the transition temperature do excitations appear; these have a 'string' nature, and they extend over distances as large as the lattice. The string picture of the SOS model is not only useful for understanding its properties, it also demonstrates the relation with six-vertex models, by interpreting the strings as paths of inverted arrows with respect to the completely polarised state. Phase transitions with this type of excitations and $\alpha = \frac{1}{2}$ have been described as commensurate–incommensurate transitions (see e.g. Villain and Bak 1981, and references therein) or as Pokrovsky–Talapov (1979) transitions. To our knowledge the first example was, however, the KDP model solved by Wu (1968). He showed that this model was equivalent to a dimer model on the honeycomb lattice (which is, via the mapping given in § 2, equivalent to the SOS model investigated by Blöte and Hilhorst (1982)). Wu solved the dimer model with the Pfaffian technique introduced by Kasteleyn (1963) for dimer models.

At present we will study a more general SOS model which not only includes these three fields h_μ but also three position-dependent couplings K_ν. For the total coupling between a pair (i, j) with orientation μ we write $K_{ij} = h_\mu + K_\nu$, where the subscript ν indicates one of the three hexagonal graphs into which the bonds on the triangular lattice can be divided. The resulting total couplings K_{ij} are shown in figure 5. The K_ν have a very different nature from the fields h_μ; a sufficiently strong K_ν will favour the SOS surface to be parallel to the (1, 1, 1) plane. Hence we may expect interesting effects from the competition between the gradient fields h_μ and the sublattice fields K_ν. For the solution of this model, we make use of the diamond or dimer representation (Blöte and Hilhorst 1982). Boltzmann weights for the dimers are found by assigning the SOS energies of the erased bonds in figure 2 to the corresponding diamonds and by sharing the remaining SOS bond energies out between pairs of adjacent diamonds, each diamond representing a dimer. To this purpose, we introduce the fugacities

$$\begin{aligned} u &= \exp(-K_1+K_2+K_3) & x &= \exp(-h_1+h_2+h_3) \\ v &= \exp(+K_1-K_2+K_3) & y &= \exp(+h_1-h_2+h_3) \\ w &= \exp(+K_1+K_2-K_3) & z &= \exp(+h_1+h_2-h_3). \end{aligned} \tag{3.3}$$

The Boltzmann weight associated with a dimer is a product of two factors: one factor depends only on the orientation of the dimer and may assume the values x, y, or z; the other factor is position-dependent and may assume the values u, v, or w. Figure 6 shows these dimer weights on the honeycomb lattice. The lattice shown is rectangularly deformed in order to allow for easy site labelling with integer coordinates k and l. The sites are divided into six types as indicated in the figure. For dimer statistics on the honeycomb lattice, the boundary conditions are important. We choose a rectangular system of $K \times L$ sites with periodic boundaries. In SOS language, this

corresponds to periodic boundary conditions of the type:

$$n_{k+K,l} = n_{k,l} + \Delta_1, \qquad n_{k,L+l} = n_{k,l} + \Delta_2 \tag{3.4}$$

where Δ_1 and Δ_2 are multiples of three. Following Kasteleyn (1963), we can write the partition function of the dimer model as a linear combination of Pfaffians. In the thermodynamic limit, it is sufficient to calculate the Pfaffian of an antisymmetric $KL \times KL$ matrix $\mathbf{A}$ with elements given by

$$|A_{kl;k'l'}| = uvwxyz \exp(-2h_\mu - 2K_\nu), \tag{3.5}$$

if the sites $(k\ l)$ and $(k'\ l')$ are coupled by a bond with direction μ on the subgraph determined by ν; all other elements are zero. Furthermore, the sign of the matrix element is positive if $k' = k+1$ or $l' = l+1$, and otherwise negative. Fourier transformation converts $\mathbf{A}$ into a matrix consisting of 6×6 blocks, $\tilde{\mathbf{a}}(p,q)$, given by:

$$\tilde{\mathbf{a}}(p,q) = \tfrac{1}{3}\begin{pmatrix} -\mathrm{i}a_0 S_0 & -\mathrm{i}a_1 S_- & -\mathrm{i}a_1^* S_+ & \dots \\ -\mathrm{i}a_1^* S_- & -\mathrm{i}a_0 S_+ & -\mathrm{i}a_1 S_0 & \dots \\ -\mathrm{i}a_1 S_+ & -\mathrm{i}a_1^* S_0 & -\mathrm{i}a_0 S_- & \dots \\ a_1 C_+ & a_1^* C_0 & a_0 C_- & \dots \\ a_1^* C_- & a_0 C_+ & a_1 C_0 & \dots \\ a_0 C_0 & a_1 C_- & a_1^* C_+ & \dots \end{pmatrix} \tag{3.6}$$

with the symmetry property

$$\tilde{a}_{ij}(p,q) = -\tilde{a}_{7-i,7-j}(p,q), \qquad i,j = 1,2,\dots,6 \tag{3.7}$$

and with

$$\begin{aligned} S_0 &= x \sin p + (y+z)\sin q & a_0 &= u+v+w \\ S_\pm &= x \sin p + (y+z)\sin(q \pm 2\pi/3) & a_1 &= u+\beta v+\beta^* w \\ C_0 &= x \cos p - (y-z)\cos q & \beta &= \exp(2\pi \mathrm{i}/3). \\ C_\pm &= x \cos p - (y-z)\cos(q \pm 2\pi/3) \end{aligned}$$

The angles p and q assume the values (K, L even)

$$p = (\pi/K)(0,1,\dots,K-1), \qquad q = (2\pi/3L)(0,1,\dots,L-1).$$

Because of its symmetry property, the effective size of $\tilde{\mathbf{a}}$ can be further reduced. Define a matrix

$$\mathbf{K} = \frac{1}{\sqrt{2}}\begin{pmatrix} \mathbb{1} & \mathbb{1} \\ \mathbf{R} & -\mathbf{R} \end{pmatrix} \tag{3.8}$$

where the submatrices are of size 3×3, and

$$R_{ij} = \delta_{i,4-j} \qquad i,j = 1,2,3.$$

It follows easily that

$$\mathbf{K}^{\mathrm{T}} \cdot \tilde{\mathbf{a}} \cdot \mathbf{K} = \begin{pmatrix} \mathbf{0} & \mathbf{A}_{12} \\ \mathbf{A}_{21} & \mathbf{0} \end{pmatrix} \tag{3.9}$$

with

$$\mathbf{A}_{12}=\tfrac{1}{3}\begin{pmatrix} -ia_0S_0+a_0C_0 & -ia_1S_-+a_1C_- & -ia_1^*S_++a_1^*C_+ \\ -ia_1^*S_-+a_1^*C_- & -ia_0S_++a_0C_+ & -ia_1S_0+a_1C_0 \\ -ia_1S_++a_1C_+ & -ia_1^*S_0+a_1^*C_0 & -ia_0S_-+a_0C_- \end{pmatrix} \tag{3.10}$$

and $\mathbf{A}_{21}=-\mathbf{A}_{12}^{\dagger}$.

If we use that $\mathrm{Pf}\,\mathbf{A}=(\det\mathbf{A})^{1/2}$, and that the determinant is invariant under the applied transformations, the free energy per site f of the TISOS model in the thermodynamic limit follows, after some algebra, as:

$$f=\frac{2}{KL}\lim_{K,L\to\infty}\log Z=\frac{1}{24\pi^2}\int_0^{2\pi}\mathrm{d}p\int_0^{2\pi}\mathrm{d}q\,\log(|s\,\mathrm{e}^{\mathrm{i}p}+t\,\mathrm{e}^{3\mathrm{i}p}-t_y\,\mathrm{e}^{-3\mathrm{i}q}+t_z\,\mathrm{e}^{3\mathrm{i}q}|^2) \tag{3.11}$$

with

$$s=(u^3+v^3+w^3)xyz, \qquad t=uvwx^3, \qquad t_y=uvwy^3, \qquad t_z=uvwz^3.$$

One easily sees that f is equal to $\frac{1}{3}\log t$ plus a function of $(u^3+v^3+w^3)/uvw$, y/x, and z/x. Thus we have solved what is effectively a three-parameter model.

4. Phase diagram and critical behaviour

The criticality condition of the TISOS model is related to the occurrence of zeros in the expression between absolute value signs in (3.11). Thus we require the real and imaginary parts to be simultaneously equal to zero:

$$s\cos p+t\cos 3p-t_-\cos 3q=0 \tag{4.1a}$$

$$s\sin p+t\sin 3p+t_+\sin 3q=0 \tag{4.1b}$$

with $t_\pm=t_y\pm t_z$. We find that there exists a region in parameter space (s, t, t_+, t_-) where such zeros occur. The corresponding values of the coordinates (p, q) in these points generally depend on the parameters s, t, t_+ and t_-. Phase transitions are associated with hyperplanes separating regions with and without zeros in parameter space. In these critical planes, solutions of (4.1) are marginally existent; they occur at coordinates (p_0, q_0) which will appear to be constant in each critical plane. The corresponding phase transition can be investigated by expansion of (4.1) in the point (p_0, q_0). We consider four cases.

(1) $\sin p_0=\sin q_0=\pm 1$

We put $\cos p=P$, $\cos q=Q$, and expand (4.1) to second order in the small quantities P and Q:

$$(s-3t)P+3t_-Q=0 \tag{4.2a}$$

$$\tfrac{1}{2}(9t-s)P^2+\tfrac{1}{2}t_+Q^2=-s+t+t_+. \tag{4.2b}$$

Equation (4.2a) shows that P and Q are proportional; equation (4.2b) shows that solutions for small P and Q are possible when $-s+t+t_+$ is small and has the right sign. These solutions vanish in the point $(P, Q)=(0, 0)$ when $-s+t+t_+$ goes through zero, or, in the original weights,

$$(u^3+v^3+w^3)/uvw=(x^3+y^3+z^3)/xyz. \tag{4.3}$$

(2) $\sin p_0 = -\sin q_0 = \pm 1$

We put $P = \cos p$, $Q = -\cos q$. Expanding (4.1) in P and Q gives

$$(3t - s)P - 3t_- Q = 0 \tag{4.4a}$$

$$\tfrac{1}{2}(9t - s)P^2 - \tfrac{9}{2}t_+ Q^2 = -s + t - t_+ \tag{4.4b}$$

and the criticality condition is $s = t - t_+$ or

$$(u^3 + v^3 + w^3)/uvw = (x^3 - y^3 - z^3)/xyz. \tag{4.5}$$

The two remaining cases,

(3) $\cos p_0 = \cos q_0 = \pm 1$ and

(4) $\cos p_0 = -\cos q_0 = \pm 1$,

can be treated similarly. The results for criticality are

$$(u^3 + v^3 + w^3)/uvw = (-x^3 + y^3 - z^3)/xyz \tag{4.6}$$

$$(u^3 + v^3 + w^3)/uvw = (-x^3 - y^3 + z^3)/xyz. \tag{4.7}$$

Equations (4.3) and (4.5–7) can be combined into a single equation giving the whole set of critical surfaces of the system, namely

$$(u^3 + v^3 + w^3)/uvw = (ix^3 + jy^3 + kz^3)/xyz \tag{4.8}$$

with $i = \pm 1$, $j = \pm 1$, $k = \pm 1$, $ijk = +1$.

In figure 7 we show the critical lines for the case where $v = w$ and $y = z$. The first condition does, in fact, not imply loss of generality because the model depends on u, v and w effectively only through one parameter. Equation (4.3) is represented by the two lines separating phases F and R (standing for flat and rough, as we shall show in the subsequent discussion). The third line represents equation (4.5) and is the boundary of the flat phase X. Two other phases, to be labelled Y and Z, form a triplet together with X, but are not visible in this figure since the critical surfaces given by (4.6) and (4.7) do not intersect with the plane of figure 7.

The expansion in the variables P and Q such as given above for the determination of the boundaries of the F phase can also be used to find the leading critical behaviour

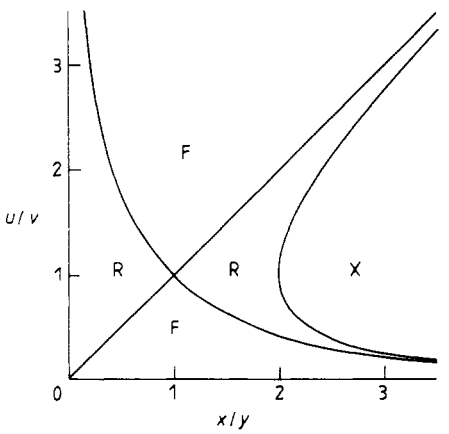

Figure 7. Phase diagram of the TISOS model for the case $y = z$ and $v = w$. The two critical lines between R (rough) and F (flat) phases follow from equation (4.3). The critical line between the R and X phases follows from equation (4.5).

near this boundary. This is done in appendix 1. The result is given in terms of f_s, the singular part of the free energy per site, and the temperature parameter Δ defined as $\Delta = s - t - t_+$:

$$\begin{aligned} &\partial f_s/\partial\Delta - (\partial f_s/\partial\Delta)_{\Delta=0} = 0 && \text{if } \Delta \geqslant 0, \\ &\partial f_s/\partial\Delta - (\partial f_s/\partial\Delta)_{\Delta=0} \sim (-\Delta)^{1/2} && \text{if } \Delta \leqslant 0. \end{aligned} \tag{4.9}$$

The specific heat like quantity $c_\Delta = \partial^2 f_s/\partial\Delta^2$ behaves in a non-singular way in the F phase. However, it diverges as

$$c_\Delta \sim 1/(-\Delta)^{1/2} \tag{4.10}$$

in the R phase when the boundary with the F phase is approached. Note that we have assumed $s \neq 3t$ in appendix 1; if this assumption does not hold, we may still obtain the results (4.9) and (4.10) provided $t_- \neq 0$ (by integrating first over Q in equation (A1.2)).

The case $s = 3t$ and $t_- = 0$ in the critical surface is special: it is important how the critical point is approached. We first consider the case $t = t_y = t_z$ (the line $x/y = 1$ in figure 7). This is worked out in appendix 1. The singularity in the free energy is found to obey

$$\partial f_s/\partial\Delta - (\partial f_s/\partial\Delta)_{\Delta=0} \sim -\log\Delta. \tag{4.11}$$

Note that $\Delta \geqslant 0$ always for the path chosen here: we approach the critical point from the F phase. If we put $v = w = u_0$, and $u = u_0(1+\alpha)$, then $\Delta \simeq 3\alpha^2$ for small α and

$$\partial f_s/\partial u = (1/u_0)(\partial f_s/\partial\alpha) \simeq -(2\alpha\log\alpha)/(\sqrt{3}\pi u_0). \tag{4.12}$$

The second derivative of f_s with respect to u diverges logarithmically: the singularity is similar to that of the two-dimensional Ising model.

If we approach the point $x = y = z$, $u = v = w$ while $u = v = w$, the free energy does not behave singularly. In this case the model reduces to that investigated by Blöte and Hilhorst (1982); in the present notation, it has only singularities at $x = y + z$ and cyclic. A similar derivation at the boundaries of the X, Y and Z phases again shows an $\alpha = \frac{1}{2}$ singularity when the boundaries are approached from the R phase. No singularity appears on the other sides. This is in agreement with earlier results (Blöte and Hilhorst 1982) which apply to the line $u/v = 1$ in figure 7. These results indicate that phase X is flat and without excitations, and that R is a rough 'floating' phase.

For a further investigation of the character of the different phases, we make use of simplified expressions for the free energy which are derived in appendix 2. These are as follows.

(1) Phase F, $s > t + t_y + t_z$:

$$f = \tfrac{1}{3}\log(xyz) + \tilde{f}(u, v, w), \tag{4.13}$$

where $\tilde{f}$ is the reduced free energy per site when $x = y = z = 1$. It is given in appendix 2 as a function of u, v and w.

(2) Phase Y, $t_y > s + t + t_z$:

$$f = \log y + \tfrac{1}{3}\log(uvw). \tag{4.14}$$

The free energies of the X and Z phases follow simply by using symmetry arguments.

(3) Phase X, $t > s + t_y + t_z$:

$$f = \log x + \tfrac{1}{3}\log(uvw). \tag{4.15}$$

(4) Phase Z, $t_z > s+t+t_y$:

$$f = \log z + \tfrac{1}{3}\log(uvw). \tag{4.16}$$

From equations (4.13–16) we see that the free energy depends linearly on the fields h_1, h_2 and h_3 in the F, X, Y, and Z phases. The slopes of the crystal surface are constant in these phases; they correspond to the (1, 1, 1), (1, 0, 0), (0, 1, 0) and (0, 0, 1) planes of the crystal respectively. The X, Y and Z phases are characterised by the absence of thermal excitations; in the F phase local excitations do occur.

As was pointed out (see § 2), our result for the free energy determines the equilibrium shape of a crystal. More precisely, from (3.2) and (3.3) we see that the quantity

$$\tilde{f} = f - \tfrac{1}{3}\log(xyz) \tag{4.17}$$

describes this shape. Figure 8 shows a (1, 1, 1) corner of a crystal for the case that u, v and w are not equal (the case $u = v = w$ was shown in figure 1). The appearance of the (1, 1, 1) facet is a consequence of this inequality.

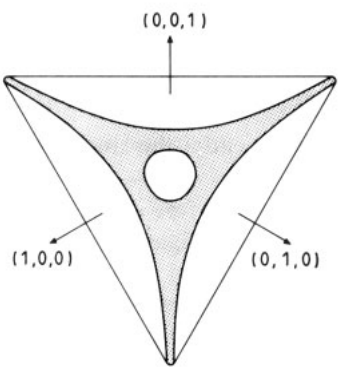

Figure 8. An equilibrium crystal shape according to the TISOS model, for the case that not $u = v = w$. For $u = v = w$, the (1, 1, 1) facet disappears (see figure 1). The curved part of the crystal surface is shown by the shaded area.

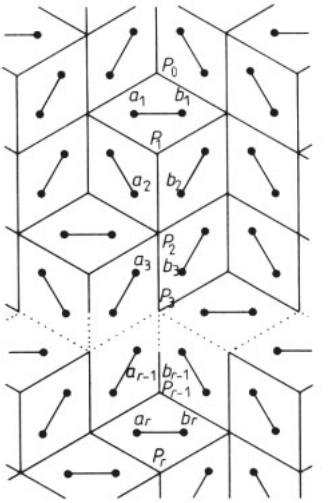

Figure 9. Illustration of the calculation of the height–height correlation function via dimer occupation numbers. The equivalence of the dimer and SOS models is shown in § 2.

5. Height–height correlation functions

A result for the height–height correlation function was given for the case $x = y = z$, $u = v = w$ by Blöte and Hilhorst (1982). Here we present a calculation for the more general case $u = v = w$. This parameter subspace intersects the X, Y, Z and R phases, but not the F phase. The first step is to express height differences in dimer occupation numbers. This procedure is illustrated with the help of figure 9, in which a typical SOS configuration is shown, together with the associated dimer configuration on the dual lattice. The mappings given in § 2 relate the height difference $h_i - h_{i-1}$ between sites P_i and P_{i-1} to the dimer occupation number N_i of sites a_i and b_i, where the

nearest-neighbour pair (a_i, b_i) is dual to the pair (P_i, P_{i-1}):

$$n_i - n_{i-1} = 3N_i - 1. \tag{5.1}$$

The height–height correlation function

$$g(r) = \langle [(n_r - n_0) - \langle n_r - n_0 \rangle]^2 \rangle \tag{5.2}$$

can now be written

$$g(r) = 9 \sum_{i=1}^{r} \sum_{j=1}^{r} \Big(\langle N_i N_j \rangle - \langle N_i \rangle \langle N_j \rangle \Big). \tag{5.3}$$

These expectation values follow by differentiation of the partition function:

$$g(r) = 9 \sum_{i=1}^{r} \sum_{j=1}^{r} \frac{\partial^2 \log Z(K_i, K_j)}{\partial K_i \, \partial K_j} \tag{5.4}$$

where K_i is the reduced energy associated with a dimer covering sites a_i and b_i; at present, $\exp(-K_i) = z$. The next step is to calculate $Z(K_i, K_j)$ when K_i and K_j are allowed to differ infinitesimally from $\log z$. The partition function of this slightly perturbed model is written as the Pfaffian of an antisymmetric matrix $\mathbf{A}$. Let $\mathbf{A}_0$ be the matrix for the uniform model (defined in § 3, $K_i = K_j = -\log z$); then we may write the matrix for the model with different K_i and K_j as

$$\mathbf{A} = \mathbf{A}_0 + \mathbf{A}_1 \tag{5.5}$$

where $\mathbf{A}_1$ is a matrix with only few non-zero elements. One finds

$$\left(\frac{\partial^2 \log Z}{\partial K_i \, \partial K_j} \right)_{K_i = K_j = -\log z} = \frac{1}{2} \frac{\partial}{\partial K_i} \frac{\partial}{\partial K_j} \det(\mathbf{A}') - \frac{1}{2} \frac{\partial}{\partial K_i} \det(\mathbf{A}') \frac{\partial}{\partial K_j} \det(\mathbf{A}')$$

with $\mathbf{A}' = \mathbb{1} + \mathbf{A}_0^{-1} \cdot \mathbf{A}_1$.

$\mathbf{A}'$ has only few columns with non-zero off-diagonal elements. For this reason, it reduces to a tractable effective size. Further, $\mathbf{A}_0$ can be inverted without difficulty and after some algebra one obtains

$$\partial^2 \log Z / \partial K_i \, \partial K_{i+n} = [\cos(2n\omega_c) - 1] / 2\pi^2 n^2 \tag{5.6}$$

with

$$\omega_c \equiv \cos^{-1}[(x^2 - y^2 - z^2)/2yz] \tag{5.7}$$

where we have supposed $x \geqslant y$ and $x \geqslant z$.

Equation (5.6) applies to $n = 1, 2, \ldots$. The case $n = 0$ is special and yields

$$\partial^2 \log Z / \partial K_i^2 = \omega_c / \pi - \omega_c^2 / \pi^2. \tag{5.8}$$

If $x > y + z$ (so that there is no solution for ω_c), then the system is flat, and $g(r) = 0$.

Substituting (5.7) and (5.6) into (5.4), we obtain

$$g(r) = 9r \left(\frac{\omega_c}{\pi} - \frac{\omega_c^2}{\pi^2} \right) \frac{9}{\pi^2} \sum_{j=1}^{r} \frac{(r-j)[\cos(2j\omega_c) - 1]}{j^2}. \tag{5.9}$$

We make use of the following expansions:

$$\sum_{j=1}^{r} \frac{1}{j^2} = \frac{\pi^2}{6} - \frac{1}{r} + \frac{1}{2r^2} - \frac{1}{6r^3} + \ldots \tag{5.10}$$

$$\sum_{j=1}^{r} \frac{1}{j} = \gamma + \log r + \frac{1}{2r} - \frac{1}{12r^2} + \ldots \tag{5.11}$$

$$\sum_{j=1}^{r} \frac{\cos(jx)}{j^2} = \frac{1}{4}x^2 - \frac{1}{2}\pi x + \frac{1}{6}\pi^2 - \frac{1}{2}\frac{\cos[(r+1)x]-\cos(rx)}{1-\cos x}\frac{1}{r^2} - \frac{\cos(rx)}{1-\cos x}\frac{1}{r^3} + \ldots \tag{5.12}$$

$$\sum_{j=1}^{r} \frac{\cos(jx)}{j} = -\frac{1}{2}\log(2-2\cos x) - \frac{\cos[(r+1)x]-\cos(rx)}{2(1-\cos x)}\frac{1}{r} - \frac{\cos(rx)}{2(1-\cos x)}\frac{1}{r^2} + \left(\frac{\cos(rx)-\cos[(r-1)x]}{2(1-\cos x)^2} - \frac{\cos(rx)}{2(1-\cos x)}\right)\frac{1}{r^3} + \ldots \tag{5.13}$$

For equations (5.10) and (5.11) see e.g. Rottmann (1960); equations (5.12) and (5.13) can be derived by substitution of $\int_0^\infty \mathrm{d}p\, p^{i-1}\, \mathrm{e}^{-pj}$ for j^{-i} $(i=1,2)$, execution of the summations, and expansion of the integrals.

Substitution in equation (5.9) gives

$$g(r) = (9/\pi^2)[\log(2r\sin\omega_c) + \gamma + 1 + (\tfrac{1}{12} - \cos(2r\omega_c)/4\sin^2\omega_c)/r^2 + \ldots]. \tag{5.14}$$

Hence, the system is rough if $x < y+z$ $(x \geqslant y, x \geqslant z)$. The deviations from flatness behave as $(\log r)^{1/2}$ for large r, just as in the Gaussian (Knops 1977, José *et al* 1977) and BCSOS (van Beijeren 1977) models. Remarkably, the coefficient does not depend on the fugacities x, y and z. Since the X, Y and Z phases do not have thermal excitations, it follows that they have zero deviation from flatness. This conclusion does not apply to the F phase, which does have thermal excitations. However, these local excitations cannot affect the global slope of the surface. This is evident from the free energy (4.14) which depends (via x, y and z) linearly on the fields h_1, h_2 and h_3: there is a plane facet of non-zero extent. This provides evidence that the F phase is smooth, i.e. $g(r)$ remains finite when $r \to \infty$. On the other hand, the dependence of the free energy (3.11) in the R phase is such that the slope of the surface varies with the fields: the crystal surface is rounded. This, together with the result (5.14), demonstrates that the R phase is rough.

6. Correspondence between Ising and TISOS operators

The equivalence between the zero-temperature antiferromagnetic triangular Ising model and the TISOS model (Blöte and Hilhorst 1982) can be utilised in two directions. It is possible to work out the exact solution of the Ising model to make predictions for the equivalent TISOS model (and thus for a cubic crystal shape). Here we work the other way: using known properties of SOS models we calculate some new properties of the triangular Ising model.

The critical behaviour of SOS models is usually formulated in terms of spin-wave and vortex operators (José *et al* 1977). Here we give a summary of the main results; for a more extensive discussion the reader is referred to a recent review (Nienhuis 1984). By a spin-wave operator we mean in this context an interaction term of the form

$$S_p \sum_j \cos(2\pi n_j/p), \tag{6.1}$$

where p is the period of the spin wave. In the rough phase there are critical phenomena associated with such terms, which can be observed for instance in the singular dependence of the free energy on S_p,

$$f \sim |S_p|^{2/Y_p^{(s)}} \tag{6.2}$$

asymptotically for small values S_p. The exponent is given by

$$Y_p^{(s)} = 2 - T_R/2p^2. \tag{6.3}$$

The renormalised temperature, T_R, is the ultimate value of the temperature of the SOS model as it reduces to a Gaussian model under renormalisation (José *et al* 1977, Nienhuis 1984). For most SOS models T_R cannot be calculated exactly. The main value of equation (6.3) lies in the specific dependence on p, which yields exact relations between the exponents of different spin waves, even when the exponents themselves are not known exactly.

Equation (6.2) is valid only when $Y_p^{(s)} > 0$. In this case the spin wave is called relevant and a non-zero value of S_p causes a transition to a smooth phase. Of both relevant and irrelevant spin waves the correlation function decays algebraically for large distances:

$$\langle \cos[(2\pi/p)(n_j - n_k)] \rangle \sim |r_{jk}|^{-2X_p^{(s)}}, \tag{6.4}$$

with $X_p^{(s)} = 2 - Y_p^{(s)}$, and r_{jk} being the distance between the sites j and k.

In the SOS model language the spin-wave and vortex operators do not seem much alike. They are however related by duality (José *et al* 1977). Let an SOS model be defined by means of the height gradient ∇n rather than n itself. Only when ∇n is a conservative field is it possible to define the height variables from their gradient. A configuration of ∇n which has zero curl everywhere except in a single face of the lattice, is a configuration of an isolated vortex. The value of the curl at the singular face is the strength of the vortex. Let the SOS partition sum be calculated over configurations including those with vortices, such that the density of vortices of strength q is controlled by a fugacity V_q. Then the free energy of the SOS model in the rough phase depends singularly on V_q as

$$f \sim |V_q|^{2/Y_q^{(v)}}. \tag{6.5}$$

The exponent is given by an equation similar to (6.3)

$$Y_q^{(v)} = 2 - q^2/2T_R. \tag{6.6}$$

The renormalised temperature T_R of the TISOS model can be calculated from the amplitude of the height–height correlation function (5.14). Taking the second derivative of the spin-wave correlation function, (6.4), with respect to $1/p$, in the limit $p \to \infty$ yields the equation

$$\langle (n_j - n_k)^2 \rangle \sim (T_R/2\pi^2) \log(r_{jk}). \tag{6.7}$$

From equation (5.14) it then follows that

$$T_R = 18. \tag{6.8}$$

Thus being provided with the value of T_R, we now know the exponents of all spin-wave and vortex operators.

In order to make the above equations applicable to the TISOS model and ultimately to the Ising model, we inspect the correspondence between the two models in more detail. Figure 3 shows the triangular lattice divided into three sublattices, labelled 0, 1 and 2. Recall that the height variables on sublattice j can assume values equal to j plus an integer multiple of three. On adjacent sites parallel Ising spins correspond to

a height difference of two, and antiparallel spins to a difference of one. We adopt the convention that even and odd values of the height are associated with Ising variables equal to +1 and −1 respectively:

$$\sigma_j = \cos(\pi n_j). \tag{6.9}$$

Thus a height variable, already limited by the sublattice it sits on, is further constrained by the value of the Ising spin, and thus determined up to a multiple of six. This fact is illustrated by table 1, which lists the six possible Ising configurations of an elementary triangle of the lattice together with corresponding TISOS configurations.

Table 1. Ising and corresponding TISOS configurations of an elementary triangle. Each TISOS configuration is obtained from the one preceding in the list, by increasing the smallest of the three height variables by 3, so that the average height is increased by 1. The corresponding Ising configuration follows from equation (6.9). After six levels in the TISOS model the same Ising state recurs.

	TISOS	Ising
Sublattice	0 1 2	0 1 2
Average height		
1	0 1 2	+ − +
2	3 1 2	− − +
3	3 4 2	− + +
4	3 4 5	− + −
5	6 4 5	+ + −
6	6 7 5	+ − −
7	6 7 8	+ − +
8	9 7 8	− − +

The parameters K_1, K_2 and K_3, introduced in § 3, play the role of intersublattice coupling constants between the sublattices 1–2, 2–0 and 0–1 respectively. If $K_1 < K_2 = K_3$, the configurations in table 1 with average height 3 and 6 are energetically favourable over the others, because in these states the sublattices that are most strongly coupled are the least separated in height. The same of course applies to any TISOS configuration in which the average height of an elementary triangle is a multiple of three. This effect is precisely that of a spin-wave term (6.1) with period 3. Therefore it may be expected as in equation (6.2) that the free energy is a singular function of $2K_1 - K_2 - K_3$, with an exponent $Y_3^{(s)} = 1$. This is indeed confirmed by the solution of the corresponding Ising model.

A coupling H of the Ising spins to a magnetic field introduces a probability difference between even and odd valued heights. This follows directly from the definition of the Ising spin, (6.9), and is also evident from table 1. Therefore the Ising magnetic field corresponds to a spin wave with period 2 in the TISOS model. The exponent then follows immediately from substituting (6.8) into (6.3): $Y_2^{(s)} = -\frac{1}{4}$. This result implies, unexpectedly, that the magnetic field in the antiferromagnetic triangular Ising model is irrelevant. Therefore the zero-temperature criticality is not destroyed by infinitesimal values of the field H, which can only order the model at some finite

value H_c. The critical value of the physical magnetic field $B_c = H_c k_B T_{Is}$, however, vanishes at zero Ising temperature T_{Is}. Since H_c approaches a non-zero constant as T_{Is} vanishes, B_c approaches zero linearly in T_{Is}. This behaviour was found numerically by Kinzel and Schick (1981), but believed by them to be an inaccuracy of their numerical method. They expected B_c to vanish exponentially with T_{Is}. Sometimes our numerical techniques are better than our beliefs.

Now let us introduce a staggered field in the Ising model, which induces the spins on sublattice 0 to be +1 and on sublattice 1 and 2 to be −1. This favours every sixth level of the TISOS model and thus corresponds to a spin wave with period 6. Therefore the associated critical exponent is $X_6^{(s)} = \frac{1}{4}$, in agreement with the results of Stephenson (1970). Based on the exponents of the magnetic and the staggered field the most dominant parts of the Ising spin–spin correlation function behave as

$$\langle \sigma_j \sigma_k \rangle \sim A r_{jk}^{-1/2} \cos[(2\pi/3) r_{jk}] + B r_{jk}^{-9/2} \tag{6.10}$$

asymptotically for large values of the distance r_{jk} between the sites j and k. The oscillatory term here is given for the case that j and k are separated by a vector parallel to a nearest-neighbour bond. For general separation it is a function equal to 1 if j and k are on the same sublattice and $-\frac{1}{2}$ otherwise. Both the oscillatory and the monotonic part may in addition have correction-to-scaling contributions that decay with larger powers of r_{jk}. From the equivalence with the TISOS model we cannot predict the values of A and B.

Thus far we have always considered the Ising model at zero temperature. It is possible however to express the Ising temperature variable in SOS terms. Besides the six possible configurations of an elementary triangle listed in table 1, at finite T_{Is} the three spins can also be all up or all down. The implication is clearly visible in figure 2. In the direction of the arrows the value of ∇n is −2 at all three sides. This is clearly not a possible SOS configuration. In fact it is a vortex of strength 6, since after a closed walk round the triangle there is a mismatch in the height of 6. The fugacity of these vortices is $\exp(2J)$, in which J is the nearest-neighbour Ising coupling constant. Therefore this parameter is relevant with exponent $Y_6^{(v)} = 1$, in agreement with Houtappel's (1950) solution. The vortices in the TISOS model correspond to dislocations in the crystal surface. However, they are in thermal equilibrium with other surface excitations. In real crystals surface dislocations constitute the end points of dislocation lines in the bulk, which, as far as the surface is concerned, should be considered as quenched.

An important drawback of the solution for the crystal shape as obtained from the triangular Ising model, is the fact that there is no parameter to vary the TISOS temperature. Varying the temperature of the crystal does not necessarily correspond to varying the prefactor of the Hamiltonian in the partition sum. It is however possible to find a parameter in the Ising model that has the intuitive effect of a temperature in the TISOS model. A second-neighbour pair of Ising spins which are parallel correspond to equal heights. If the Ising spins are antiparallel the heights differ by 3. Therefore introducing a ferromagnetic second-neighbour coupling in the triangular Ising model is like lowering the temperature of the TISOS model. Unfortunately the Ising model with first- and second-neighbour coupling has not been solved, and can therefore be of no use in understanding the TISOS model. However, since a number of Ising operators have now been identified as spin-wave and vortex operators, the dependence of their exponents on T_R is known, and can be utilised to study the Ising model.

7. The Ising phase diagram and the crystal shape

Figure 10 shows a qualitative picture of the phase diagram of the triangular antiferromagnetic Ising model with first- and second-neighbour coupling J and L, and coupling to a magnetic field H. Critical sections of the phase diagram are indicated by the shaded planes and the heavy segment of the L axis. The parameter $\exp(2J)$ will be loosely referred to as (Ising) temperature, since $\exp(2J)=0$ corresponds to zero temperature. The thermal and magnetic exponents, Y_T and Y_H, associated with $\exp(2J)$ and H respectively, are as derived above

$$Y_T = 2 - 18/T_R, \qquad Y_H = 2 - T_R/8. \tag{7.1a, b}$$

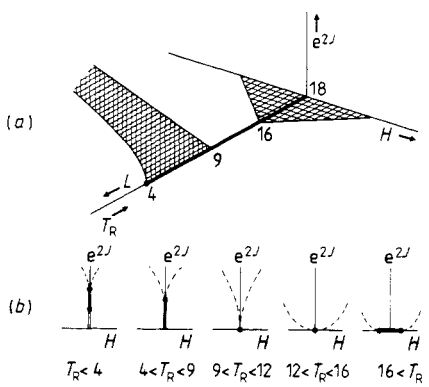

Figure 10. Phase diagram of the antiferromagnetic triangular Ising model with first- and second-neighbour interaction J and L, respectively, and magnetic field H. In (a) the boldly drawn segment of the L-axis and the shaded regions of the L–H plane and of the L–e^{2J} plane mark transitions with continuously varying exponents. Other transitions are not shown here. In (b) some intersections of the phase diagram at fixed values of L are given. The heavy lines again indicate transitions with continuously varying exponents, the broken curves transitions with three-state Potts exponents and the double line a first-order transition. The way in which the various transition lines meet, follows from RG arguments.

The origin $\exp(2J)=L=H=0$ corresponds to the isotropic point $u=v=w$ and $x=y=z$, of the exact solution in § 3. At this point, since $T_R=18$, the magnetic field is irrelevant, so that the model remains critical for finite values of H. If the field is sufficiently strong, however, the model orders into one of the three phases where two sublattices are up and one is down. The Ising temperature is relevant with exponent 1.

We now let the second-neighbour coupling L increase, so that T_R decreases. The first qualitative change happens at $T_R=16$, where H becomes relevant, and the critical range of H vanishes as a consequence. The next event is at $T_R=9$, where the temperature becomes irrelevant, so that beyond this point the Ising model remains critical up to some finite temperature, terminating in a Kosterlitz–Thouless (1973) transition. Finally, at $T_R=4$, the spin wave with period 1, which is present in the TISOS model proper, causing the heights to be integral, becomes relevant as well. For larger values of L, when $T_R<4$, the TISOS model is no longer rough, and correspondingly the Ising model here has an ordered low-temperature phase, at which the field causes a first-order transition. This ordered phase is separated from the high-temperature

phase by a finite critical regime. This latter phase pattern corresponds with the generally accepted idea that this Ising model is in the six-state clock universality class (José *et al* 1977). However the way in which this diagram emerges as the second-neighbour coupling increases, was not known previously. In particular, as evident from figure 10, the zero-temperature critical point of the antiferromagnetic nearest-neighbour triangular Ising model ($T_R = 18$), does not correspond to the upper ($T_R = 9$) or lower ($T_R = 4$) transition of the six-state clock model, nor even to a point in between.

The spin-wave and vortex operators have thus been shown to be equivalent to some simple quantities in the Ising model. Another question is their physical meaning for actual crystal shapes. In some alkali halogenides like NaCl the two species of ions form two interpenetrating FCC lattices, which together make up an SC lattice. It can be thought of as built up, in the (1, 1, 1) direction, of layers, consisting alternately of Na^+ and Cl^- ions. Suppose the crystal is in equilibrium with a melt or solution with an excess of Na^+ ions, electrically compensated by large negative ions, which due to their size cannot easily be implemented as defects in the NaCl lattice. Then it will be statistically favourable for the crystal that the exposed surface consists of Na^+ ions rather than Cl^-. This difference in chemical potential between the two species of ions is thus a physical realisation of the spin wave with period 2, in the TISOS model, and of a magnetic field in the corresponding Ising model.

The spin wave with period 3 can be realised in slightly more complicated crystals, consisting of three species of ions in equal numbers. They can be built up as follows. Take a triangular lattice of ions of species 1 in the base plane. Ions of species 2 are deposited straight above the left-pointing triangles of the first lattice. Likewise ions of species 3 are deposited straight above the left-pointing triangles of species 2, and so on in cyclic order. The resulting three-dimensional lattice is then like a simple cubic lattice, in which three sublattices are populated by different ions. Possibly the lattice structure is stretched or compressed in the (1, 1, 1) direction. The surface of the crystal can be described by a TISOS model with the three sublattices coupled unequally. A difference in concentration of the constituent ions in the melt or solution with which the crystal is in equilibrium, has the effect of a spin wave with period 3, since the exposed surface will prefer to consist of the most abundant ions.

In the solution of the TISOS model, discussed in § 4, a (1, 1, 1) facet appears with a radius proportional to $u - v$ (see figure 7), that is for the actual crystal proportional to the mismatch in concentration of the three species of ions. This, however, cannot be expected to hold generally at all temperatures of the crystal. The way in which the phase boundaries in figure 7 approach the point (1, 1) is governed by the ratio of the exponent of $u - v$ and that of $x - y$. When the temperature is varied, T_R changes and the exponent of $u - v$ varies as $Y_3^{(s)}$ according to equation (6.3). The exponent of $x - y$ however does not change, but remains equal to 1, since x and y couple to ∇n. Therefore the (1, 1, 1) facet appears with a radius R_f

$$R_f \sim \mu^{1/Y_p^{(s)}} \tag{7.2}$$

where μ is the excess concentration of one of the species, and $p = 3$. For crystals of the NaCl type the same equation holds with $p = 2$. The exponent $Y_p^{(s)} < 2$, but is not otherwise constrained. When $Y_p^{(s)} < 0$ the facet appears only at non-zero values of μ via a Kosterlitz-Thouless (1973) transition.

When $\mu = 0$, i.e. in a cubic crystal with no distinction between the sublattices, the (1, 1, 1) facet can appear spontaneously, as the temperature is lowered beyond $T_R = 4$.

This also happens via a Kosterlitz–Thouless transition (compare Jayaprakash *et al* 1983).

8. Conclusion

We summarise the results of the previous sections. There are four flat phases in the TISOS model. These correspond to the (1, 0, 0), (0, 1, 0), (0, 0, 1) and (1, 1, 1) facets of a cubic crystal. There is one rough phase in the TISOS model; it corresponds to the curved part of the crystal surface, which separates the flat parts. Criticality of the TISOS model corresponds to the boundary lines on the crystal surface between the flat and curved parts. The critical behaviour of the TISOS model is of the commensurate–incommensurate (Pokrovsky–Talapov) type. As a consequence, close to the flat facets, the slope of the curved part of the surface behaves as the square root of the distance to the boundary of the facet. This is in agreement with the behaviour found for related models (see e.g. Jayaprakash *et al* 1983, Rottman and Wortis 1984 and Zia 1983). However, the appearance of the (1, 1, 1) facet is related to a phase transition of the TISOS model with a specific heat exponent $\alpha = 0$, whereas a corresponding transition in the model investigated by Jayaprakash *et al* (1983) has $\alpha = -\infty$. This difference can be understood with the picture sketched in § 7, which contains (at zero Ising temperature) a non-universal line of critical points, with varying α.

The relevance of the TISOS model for real crystals is subject to some limitations. In the first place, the height differences in the SOS model are restricted to two possible values, and 'overhangs' are absent. However, we do not expect that the phase transitions found in our model are drastically modified by these restrictions, which pertain to the microscopic interactions between neighbouring atoms. Of course, the TISOS model only allows one to investigate the (1, 1, 1) corner of the crystal. An exact treatment of a whole crystal would require a simultaneous description of all corners, and this is outside the scope of the TISOS model.

Further, the TISOS Hamiltonian depends only on height differences between nearest neighbours; it depends on the slope of the crystal surface, but not on its curvature. This may have some consequences (Fisher and Wortis 1983, Rottman *et al* 1984) when there exists a significant curvature on an atomic length scale: such is the case right at the boundary lines of the facets in the TISOS model. However, on the macroscopic length scale considered in this work, these effects vanish.

With these limitations in mind, we can nevertheless conclude that the TISOS model, which is perhaps the simplest soluble SOS model that goes beyond mean-field theory, is rich enough to predict realistic crystal shapes.

Acknowledgments

Part of this research was supported by the Dutch 'Stichting voor Fundamenteel Onderzoek der Materie'. Instructive conversations with Professors J M J van Leeuwen, M Wortis and R K P Zia are gratefully acknowledged.

Appendix 1. Critical behaviour near the phase boundaries

The singular part of the reduced free energy f_s can only arise from integration (equation 3.11) in the neighbourhood of the point p_0, q_0. We first consider the boundaries of the

F phase. Thus, for small $|s-t-t_+|$,

$$f_s=(1/12\pi^2)\iint \mathrm{d}P\,\mathrm{d}Q\,\log\{[(s-3t)P+3t_-Q]^2 + [s-t-t_+ +\tfrac{1}{2}(9t-s)P^2+\tfrac{1}{2}t_+Q^2]^2\}. \tag{A1.1}$$

Integration is over a region centred about the origin and with linear size δ chosen such that $|s-t-t_+|\ll\delta\ll 1$. If $s\neq 3t$, one can substitute

$$P=R-[3t_-/(s-3t)]Q$$

yielding

$$f_s=(1/12\pi^2)\int_{-\delta}^{\delta}\mathrm{d}Q\int_{-\delta}^{\delta}\mathrm{d}R\,\log\{AR^2+[\Delta+B(CR+Q)^2+\tfrac{1}{2}t_+Q^2]^2\} \tag{A1.2}$$

where

$$\Delta=s-t-t_+$$

represents the distance from criticality, and

$$A=(s-3t)^2,\qquad B=\tfrac{9}{2}(9t-s)t_-^2/(s-3t)^2,\qquad C=(s-3t)/3t_-.$$

The term CR in expression (A1.2) is never dominant and can be neglected. Thus

$$f_s=(1/12\pi^2)\int_{-\delta}^{\delta}\mathrm{d}Q\int_{-\delta}^{\delta}\mathrm{d}R\,\log[AR^2+(\Delta+DQ^2)^2] \tag{A1.3}$$

where $D=\frac{1}{2}B+\frac{1}{2}t_+$ is always positive on the critical surface. Differentiation with respect to Δ gives

$$\frac{\partial f_s}{\partial\Delta}=\frac{1}{6\pi^2}\int_{-\delta}^{\delta}\mathrm{d}Q\frac{\Delta+DQ^2}{A}\int_{-\delta}^{\delta}\mathrm{d}R\frac{1}{R^2+(\Delta+DQ^2)^2/A}. \tag{A1.4}$$

The integration over R can be carried out. Using $\delta\gg\Delta$ and $\delta\gg Q^2$,

$$\frac{\partial f_s}{\partial\Delta}=\frac{1}{6\pi}\int_{-\delta}^{\delta}\frac{\mathrm{d}Q}{\sqrt{A}}\,\mathrm{sgn}(\Delta+DQ^2). \tag{A1.5}$$

Thus

$$\begin{aligned}&\partial f_s/\partial\Delta-(\partial f_s/\partial\Delta)_{\Delta=0}=0 \qquad \text{if } \Delta\geqslant 0\\ &\partial f_s/\partial\Delta-(\partial f_s/\partial\Delta)_{\Delta=0}\simeq-(1/3\pi)(-\Delta/AD)^{1/2} \qquad \text{if } \Delta\leqslant 0.\end{aligned} \tag{A1.6}$$

The second derivative with respect to Δ is (if $s\neq 3t$) singular only for $\Delta\uparrow 0$:

$$\partial^2 f_s/\partial\Delta^2\simeq[6\pi(-AD\Delta)^{1/2}]^{-1}. \tag{A1.7}$$

However, for $s=3t$, there exists one point on the F phase boundary where f behaves singularly for $\Delta\downarrow 0$: the symmetry point $u=v=w$, $x=y=z$. Putting $s-3t=\Delta$, $t_-=0$, $t_+=2t$ in (A1.1):

$$f_s=(1/12\pi^2)\iint \mathrm{d}P\,\mathrm{d}Q\,\log[\Delta^2P^2+(\Delta+3tP^2+tQ^2)^2]. \tag{A1.8}$$

The integration is again over a region with linear dimensions of order δ. We neglect the first term between square brackets. Substitution of $3P^2+Q^2=R^2$ and differentiation

with respect to Δ gives

$$\partial f_s/\partial\Delta = (1/3\sqrt{3}\pi)\int_0^{\delta} R\,\mathrm{d}R/(\Delta + tR^2) \tag{A1.9}$$

and

$$\partial f_s/\partial\Delta - (\partial f_s/\partial\Delta)_{\Delta=0} = -\log\Delta/6\sqrt{3}\pi t. \tag{A1.10}$$

Appendix 2. The free energy of the F and Y phases

To calculate the derivative of the free energy of phase F with respect to x we note that t_+ and t_- do not depend on x, whereas s and t do:

$$\partial f/\partial x = (1/\alpha)(s\,\partial f/\partial s + 3t\,\partial f/\partial t). \tag{A2.1}$$

After decomposing the expression between the brackets in equation (3.11) into two complex conjugate parts, one obtains

$$\frac{\partial f}{\partial x} = \frac{1}{24\pi^2 x}\int_0^{2\pi}\mathrm{d}p\int_0^{2\pi}\mathrm{d}q\,\frac{s\,\mathrm{e}^{\mathrm{i}p} + 3t\,\mathrm{e}^{3\mathrm{i}p}}{s\,\mathrm{e}^{\mathrm{i}p} + t\,\mathrm{e}^{3\mathrm{i}p} + t_y\,\mathrm{e}^{3\mathrm{i}q} - t_z\,\mathrm{e}^{-3\mathrm{i}q}} + \mathrm{CC}. \tag{A2.2}$$

Substitution of $\alpha = s\,\mathrm{e}^{\mathrm{i}p} + t\,\mathrm{e}^{3\mathrm{i}p}$ gives

$$\frac{\partial f}{\partial x} = \frac{-\mathrm{i}}{24\pi^2 x}\int_0^{2\pi}\mathrm{d}p\oint\mathrm{d}\alpha\,\frac{\mathrm{d}\alpha}{\alpha + t_y\,\mathrm{e}^{3\mathrm{i}q} - t_z\,\mathrm{e}^{-3\mathrm{i}q}} + \mathrm{CC}. \tag{A2.3}$$

The pole occurs within the path described by α in the complex plane when the condition for phase F is satisfied. Hence

$$\partial f/\partial x = 1/3x.$$

Since the model (and the condition for phase F) is symmetric in x, y and z, it follows also that $\partial f/\partial y = 1/3y$ and $\partial f/\partial z = 1/3z$.

Therefore

$$f = \tfrac{1}{3}\log(xyz) + \tilde{f}(u, v, w) \tag{A2.4}$$

in which $\tilde{f}$ is the free energy when $x = y = z = 1$. Substituting this into (3.11), one integral can be executed. After some algebra, we obtain

$$\tilde{f}(u, v, w) = \tfrac{1}{3}\log(uvw) + (2/3\pi)\int_0^{\pi/2}\mathrm{d}p\,\cosh^{-1}[(\alpha+\beta+1)/2]^{1/2} \tag{A2.5}$$

where α and β are functions of p:

$$\alpha = [(\beta+1)^2 - \gamma^2]^{1/2},$$

$$\beta = \tfrac{1}{4}[(u^3+v^3+w^3)/uvw - 1]^2 - [(u^3+v^3+w^3)/uvw]\sin^2 p.$$

$$\gamma = [(u^3+v^3+w^3)/uvw + 3]\sin p - 4\sin^3 p.$$

Also the free energy of the Y phase can be further investigated by a calculation of some of its derivatives. Differentiation of (3.11) with respect to s, and putting $\mathrm{e}^{3\mathrm{i}q} = \mu$ gives

$$\frac{\partial f}{\partial s} = -\frac{\mathrm{i}}{24\pi^2}\int_0^{2\pi}\mathrm{d}p\,\mathrm{e}^{\mathrm{i}p}\oint\frac{\mathrm{d}\mu}{\mu}\,\frac{1}{s\,\mathrm{e}^{\mathrm{i}p} + t\,\mathrm{e}^{3\mathrm{i}p} + t_z\mu - t_y/\mu} + \mathrm{CC}. \tag{A2.6}$$

Investigation of the integrand shows that there are no poles within the unit circle in phase Y (whatever the value of p). Hence we obtain

$$\partial f/\partial s = 0.$$

Similarly, we find $\partial f/\partial t = 0$ and $\partial f/\partial t_z = 0$. Differentiation with respect to t_y gives

$$\frac{\partial f}{\partial t_y} = \frac{\mathrm{i}}{24\pi^2}\int_0^{2\pi} \mathrm{d}p \oint \frac{d\mu}{\mu} \frac{1}{s\,\mathrm{e}^{\mathrm{i}p} + t\,\mathrm{e}^{3\mathrm{i}p} + t_z\mu - t_y/\mu} \frac{1}{\mu} + \mathrm{cc}. \tag{A2.7}$$

The last factor of the integrand produces a pole at $\mu = 0$; the rest of the integrand has no poles in phase Y (see (A2.6)). Thus we find

$$\partial f/\partial t_y = 1/3t_y.$$

Integration of these results shows that

$$f = \tfrac{1}{3}\log(t_y) + \text{constant}.$$

From the Hamiltonian described in § 3, we find that in the limit of large t_y, $f = \frac{1}{3}\log(t_y)$ so that the integration constant is equal to zero. Thus in phase Y

$$f = \log y + \tfrac{1}{3}\log(uvw). \tag{A2.8}$$

References

Andreev A F 1981 *Zh. Eksp. Teor. Fiz.* **80** 2042 (1982 *Sov. Phys.-JETP* **53** 1063)
Blöte H W J and Hilhorst H J 1982 *J. Phys. A: Math. Gen.* **15** L631
Fisher M P A and Wortis M 1983 *Preprint University of Illinois, Urbana-Champaign*
Houtappel R M F 1950 *Physica* **16** 425
Jayaprakash C, Saam W F and Teitel S 1983 *Phys. Rev. Lett.* **50** 2017
José J V, Kadanoff L P, Kirkpatrick S, and Nelson D 1977 *Phys. Rev.* B **16** 1217
Kasteleyn P W 1963 *J. Math. Phys.* **4** 287
Kinzel W and Schick M 1981 *Phys. Rev.* B **23** 3435
Knops H J F 1977 *Phys. Rev. Lett.* **39** 766
Kosterlitz J M and Thouless D J 1973 *J. Phys. C: Solid State Phys.* **6** 1181
Nienhuis B 1984 *J. Stat. Phys.* **34** 731
Pokrovsky V L and Talapov A L 1979 *Phys. Rev. Lett.* **42** 65
Rottman C and Wortis M 1984 *Phys. Rep.* **103** 59
Rottman C, Wortis M, Heyraud J C and Métois J J 1984 *Phys. Rev. Lett.* **52** 1009
Rottmann K 1960 *Mathematische Formelsammlung* (Bibliographisches Institut AG, Mannheim)
Stephenson J 1970 *J. Math. Phys.* **11** 413
van Beijeren H 1977 *Phys. Rev. Lett.* **38** 993
Villain J and Bak P 1981 *J. Physique* **42** 657
Wu F Y 1968 *Phys. Rev.* **168** 539
Wulff G 1901 *Z. Krist. Mineral, Petrogr.* **34** 449
Zia R K P 1983 *Proc. of the Scottish Univ. Summer School in Physics* ed K Bowler and A McKane to be published